SCIENTIFIC REPORTS

OPEN

Large gap electron-hole superfluidity and shape resonances in coupled graphene nanoribbons

Received: 07 December 2015
Accepted: 06 April 2016
Published: 25 April 2016

M. Zarenia[1], A. Perali[2], F. M. Peeters[1] & D. Neilson[2]

We predict enhanced electron-hole superfluidity in two coupled electron-hole armchair-edge terminated graphene nanoribbons separated by a thin insulating barrier. In contrast to graphene monolayers, the multiple subbands of the nanoribbons are parabolic at low energy with a gap between the conduction and valence bands, and with lifted valley degeneracy. These properties make screening of the electron-hole interaction much weaker than for coupled electron-hole monolayers, thus boosting the pairing strength and enhancing the superfluid properties. The pairing strength is further boosted by the quasi one-dimensional quantum confinement of the carriers, as well as by the large density of states near the bottom of each subband. The latter magnifies superfluid shape resonances caused by the quantum confinement. Several superfluid partial condensates are present for finite-width nanoribbons with multiple subbands. We find that superfluidity is predominately in the strongly-coupled BEC and BCS-BEC crossover regimes, with large superfluid gaps up to 100 meV and beyond. When the gaps exceed the subband spacing, there is significant mixing of the subbands, a rounding of the shape resonances, and a resulting reduction in the one-dimensional nature of the system.

Superfluidity of spatially separated electrons and holes was predicted nearly half a century ago[1] but up to now experimental observation of this exotic state has been elusive at zero magnetic field, notwithstanding multiple attempts on very different systems. The discovery of the wonder material graphene in conjunction with the large band gap insulator hexagonal boron nitride (h-BN) has raised new hopes for realization of this new collective many body state. Recently, superconductivity at temperatures above liquid Helium has been reported in doped monolayer graphene by four groups, amplifying interest in quantum coherent phenomena in graphene[2].

Monolayer graphene is an atomically flat, gapless semiconductor with near identical conduction and valence bands. Spatially separated electron-doped and hole-doped monolayers can be completely insulated from each other with just a few atomic layers of h-BN[3,4]. With such small spatial separations, electron-hole pairing by direct Coulomb attraction is expected to be strong[5–7]. However the linear dispersion of the monolayer graphene energy bands results in very strong Coulomb screening of the electron-hole pairing attraction, and this suppresses superfluidity in coupled electron-hole graphene monolayers[3,8]. To overcome the strong screening, refs 9 and 10 proposed using coupled electron-hole graphene multilayers. Using multilayers takes advantage of the nonlinear dispersion of their energy bands[11,12], and the existence of a gap between the conduction and valence bands when a gate potential is applied.

Here we propose a new design to boost electron-hole pairing and the onset of superfluidity using nanoribbons etched in monolayer graphene. Monolayer sheets of graphene are promising candidates for applications in transparent conductive films, electronic and opto-electronic devices, actuators, sensors, composites, and more. However a serious limitation of graphene monolayers is that field-effect transistor (FET) devices are not possible because the massless nature of the electrons prevents electron confinement in graphene. Quasi-one-dimensional graphene nanoribbons with tuneable band gaps resolve this issue, with important implications for the fabrication of novel and ultrafast electronic nanodevices. For example, FET devices with 100 GHz switching frequencies have been fabricated using graphene nanoribbons[13]. The nanoribbon edges can be terminated using a variety of different atoms, which opens up application opportunities, in particular for nanoribbons in polymer hosts for fabrication of novel composite materials[14,15]. Finally, graphene nanoribbons are showing great promise as electrode materials for batteries and supercapacitors[16].

[1]Department of Physics, University of Antwerp, Groenenborgerlaan 171, B-2020 Antwerpen, Belgium. [2]Dipartimenti di Fisica e di Farmacia, Università di Camerino, 62032 Camerino, Italy. Correspondence and requests for materials should be addressed to M.Z. (email: mohammad.zarenia@uantwerpen.be)

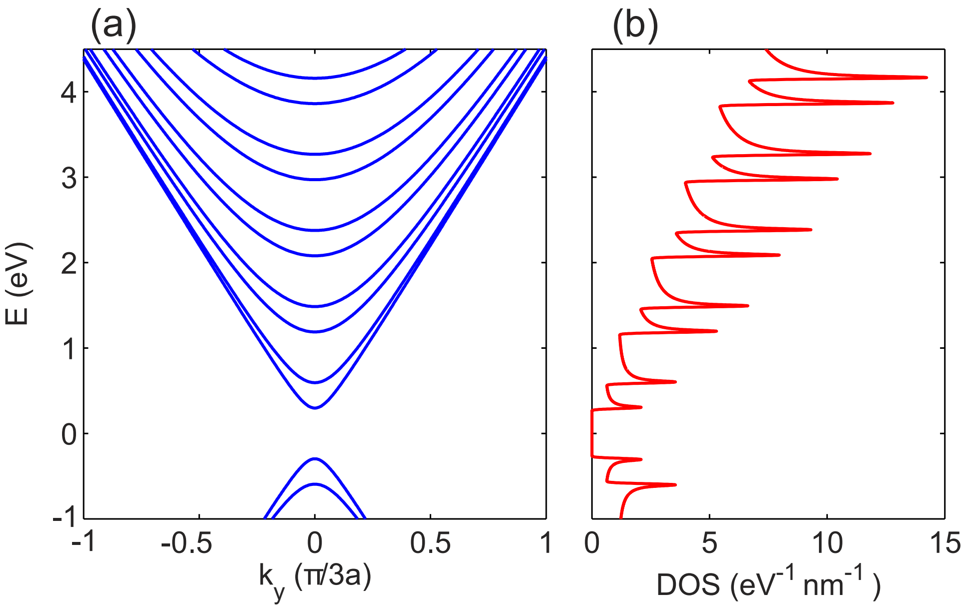

Figure 1. (**a**) Lowest single-particle energy subbands $\varepsilon_j(k_y)$, $j = 1, 2, \ldots$ in an armchair graphene nanoribbon of width $W = 2$ nm. (**b**) Corresponding density of states DOS(E) in nanoribbon. Van Hove singularities are visible at bottom of each subband.

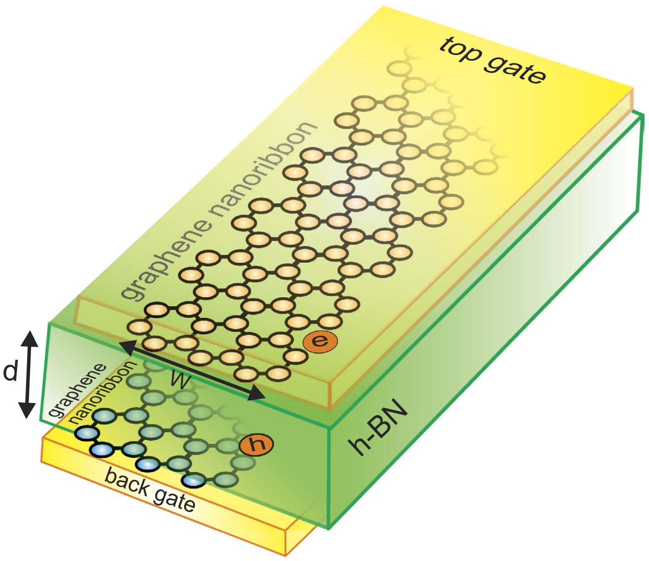

Figure 2. Proposed device. Upper electron-doped and lower hole-doped armchair-edge terminated graphene nanoribbons of widths W separated by h-BN insulator of thickness d. Top and back gates control electron and hole densities. Gates are separated from nanoribbons by h-BN layers. Nanoribbons are independently contacted.

The electronic properties of graphene nanoribbons depend on the type of edge termination[17]. We focus on armchair-edge terminated nanoribbons since (i) their subbands are parabolic around their minima (Fig. 1(a)), (ii) there is a sizeable semiconductor-like energy gap between the conduction and valence bands, and (iii) the valley degeneracy of monolayer graphene is lifted. These properties combine to greatly reduce the strength of screening of the electron-hole pairing interaction. Note that uniform armchair graphene nanoribbons of widths $W \ll 10$ nm have recently been fabricated[18].

Figure 2 shows the device we are proposing. It consists of two armchair-edge terminated monolayer graphene nanoribbons, one electron-doped and the other hole-doped, separated by a few atomic layers of a h-BN insulating barrier. The nanoribbons are independently contacted, and top and back metal gates control the carrier densities.

In addition to reducing the effect of screening, electron-hole pairing strengths will be further boosted in our proposed system by the enhanced density of states near the minimum of each subband (see Fig. 1(b)) that arises from the van Hove singularities of the quasi-one-dimensional nanoribbons, and also by the quantum confinement of the carriers in the nanoribbons. Enhancement of superconducting gaps and critical temperature in striped systems due to shape resonances and quantum confinement at the nanoscale was predicted in refs 19–21. Superconductivity has been observed in quasi-one-dimensional systems including Sn and Al metallic nanowires and carbon nanotubes, with enhanced transition temperatures as compared with their bulk values[22].

Methods

We take the y-direction parallel to the nanoribbons, with the carriers confined in the transverse x-direction. Figure 1(a) shows the single-particle energy subbands obtained in the continuum model, $\varepsilon_j(k_y) = (\sqrt{3}\,t a_0/2)\sqrt{k_y^2 + k_j^2}, j = 1, 2, \ldots$ for an armchair graphene nanoribbon of width $W = 2$ nm. The intralayer hopping energy $t = 2.7$ eV[23] and the graphene lattice constant $a_0 = 0.24$ nm. $k_j = \left|j\pi/W\right| - \left|4\pi/(3\sqrt{3}\,a_0)\right|$ is the quantized wave-number for the j-subband in the x-direction. Figure 1(b) shows the corresponding density of states DOS(E). The van Hove singularities coincide with the bottom of each subband.

Not only the finite width of the nanoribbons but also their multiple occupied subbands make the system only quasi-one-dimensional. In addition, in the superfluid state the energy gap mixes close-by subbands. The quasi-one-dimensionality together with the subband mixing will suppress order parameter fluctuations that are responsible for destroying superfluidity in a pure one-dimensional system. For these reasons we can calculate properties of the superfluid ground state using mean field theory.

Recently ref. 24 discussed a quasi-condensate of excitons in coupled electron-hole one-dimensional wires using the weak-coupled BCS gap equation in the low density limit with only the lowest subband contributing to the pairing, and with screening neglected. Since only one channel was considered, there are no shape resonance effects. Also, because of the one dimensionality, fluctuations of the order parameter should be severe and would strongly suppress superfluidity. Interestingly, ref. 24 argues that even in the one-channel case, the finite size of the nanoribbons would allow for short range superfluid correlations. In our case the many available channels due to the multiple subbands involved in the pairing allow for a suppression of the critical fluctuations, which would favour the observation of conventional long-range superfluidity.

Our calculations are for coupled electron-hole armchair graphene nanoribbons of equal width W and equal (two-dimensional) electron and hole densities $n = (r_0 W)^{-1}$, where r_0 is the average inter-particle spacing along the nanoribbon. The subbands $\varepsilon_j(k_y), j = 1, 2, \ldots$ are identical for the electrons and holes.

Because of the multiple subband structure, the zero temperature mean field equations for the superfluid state acquire an additional index for the subband j. The equations for the wave-vector dependent superfluid energy gaps $\Delta_j(k_y)$ for subbands j become,

$$\Delta_j(k_y) = -\frac{1}{L_y}\sum_{j'}^{j_c}\sum_{k'_y}^{k_c} F_{k_y j, k'_y j'} V_{\mathrm{e-h}}(k_y - k'_y)\frac{\Delta_{j'}(k'_y)}{2E_{j'}(k'_y)}, \tag{1}$$

where L_y is the nanoribbon length, $F_{k_y j, k'_y j'} = [1 + \cos(\theta_{k_y j} - \theta_{k'_y j'})]/2$ is the form factor[8] coming from the overlap of the single-particle nanoribbon wave functions, with $\theta_{k_y j} = \tan^{-1}(k_y/k_j)$, $V_{\mathrm{e-h}}(q)$ is the effective electron-hole pairing interaction, and $E_j(k_y) = [(\varepsilon_j(k_y) - \mu)^2 + \Delta_j(k_y)^2]^{1/2}$ is the single-particle energy dispersion in the superfluid state for subband j. The wave-vector k'_y is bounded by the Brillouin zone boundary $\pm k_c$. We truncate the sum over the subband index at $j' = j_c$, where j_c is the lowest subband with a minimum above the graphene nanoribbon work function energy, taken to be ~4.5 eV. The chemical potential μ is fixed by the density equation,

$$n = \frac{2}{W L_y}\sum_{j}^{j_c}\sum_{k_y}^{k_c} v_j^2(k_y), \tag{2}$$

where $v_j^2(k_y) = \frac{1}{2}[1 - (\varepsilon_j(k_y) - \mu)/E_j(k_y)]$, and the prefactor 2 is the spin degeneracy. There is no valley degeneracy for armchair graphene nanoribbons.

We neglect screening in the calculations for the following reasons. Screening is expected to be weak when the superfluid state lies in the strongly-coupled BEC or BCS-BEC crossover regimes because the superfluid gap in these regimes of pairing is comparable to the Fermi energy, resulting in a large smearing of the Fermi surface, and electron-hole pairs that are compact compared with their average spacing. This makes their mutual interactions dipolar and weakly repulsive. Similar arguments suggest in the BEC regime that electron-electron interactions between pairs will be weakened by the compensatory electron-hole interactions[25], and so we also neglect electron-electron interactions. The expected suppression of screening is confirmed by the following numerical calculations.

In the superfluid state, the RPA-like static screening polarization bubble for small qd that is responsible for screening the electron-hole pairing interaction is given by the sum,

$$\Pi_0(q) = \Pi_0^{(n)}(q) + \Pi_0^{(a)}(q), \tag{3}$$

where $\Pi_0^{(n)}(q)$ and $\Pi_0^{(a)}(q)$ are the normal and anomalous polarizabilities in the superfluid state. These are constructed from pairs of the normal and anomalous Green functions of BCS theory, respectively. The resulting expressions are[9],

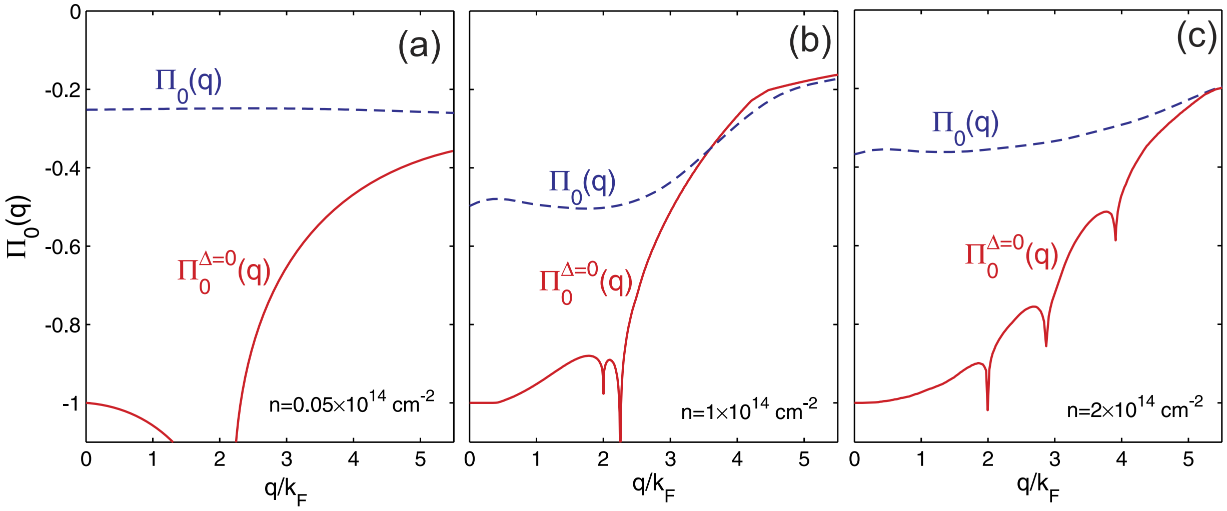

Figure 3. The polarization function $\prod_0(q)$ in the superfluid state for carrier densities n as labelled, compared with the corresponding Lindhard polarization function for the normal state of the multi-subband graphene nanoribbon, $\Pi_0^{\Delta=0}(q)$ of width $W = 2$ nm and separation $d = 3$ nm. The functions are normalized to $\Pi_0^{\Delta=0}(q = 0)$.

$$\begin{aligned}\Pi_0^{(n)}(q) &= -2\sum_{k_y jj'} F_{k_y,j,k_y-q,j'} \frac{u_j^2(k_y)v_{j'}^2(k_y - q) + v_j^2(k_y)v_{j'}^2(k_y - q)}{E_j(k_y) + E_{j'}(k_y - q)},\\ \Pi_0^{(a)}(q) &= 2\sum_{k_y jj'} F_{k_y,j,k_y-q,j'} \frac{2u_j(k_y)v_j(k_y)u_{j'}(k_y - q)v_{j'}(k_y - q)}{E_j(k_y) + E_{j'}(k_y - q)},\end{aligned} \tag{4}$$

where $u_j^2(k_y) = \frac{1}{2}[1 + (\varepsilon_j(k_y) - \mu)/E_j(k_y)]$. For convenience we write q_y as q.

The opening of the superfluid energy gap Δ at the Fermi surface exponentially suppresses particle-hole processes with energies less than Δ, and it is precisely these low-energy processes that screen the bare interaction in the normal state. As well as a suppression of the screening polarization bubble with diagonal Green functions, there is an additional cancelling contribution from the anomalous polarization bubble with off-diagonal Green functions[8]. Figure 3 compares the polarization function $\prod_0(q)$ in the superfluid state with the corresponding Lindhard polarization function for the normal state of a multi-subband graphene nanoribbon of width $W = 2$ nm and separation $d = 3$ nm. The figure shows that the presence of the superfluid gap strongly suppresses $\prod_0(q)$ for $q \lesssim 2k_F$. It is at small momentum transfers q where the unscreened electron-hole pairing interaction is peaked, and hence this suppression of screening can lead to strong pairing. For this reason we are able, to a good approximation, to neglect screening effects in the pairing interaction.

The results of Fig. 3 contain an additional interesting new phenomenon, that of a competition between superfluidity and Coulomb screening at finite momenta. For each 1D subband, the Fermi surface consists of just two discrete points $k = \pm(k_F)_i$. A consequence of this is that the static charge response in the normal state ($\Delta = 0$) diverges logarithmically when the transfer momentum q connects the two Fermi points, $q = 2(k_F)_i$ (the perfect nesting condition). The polarization bubble in the normal state will have multiple divergences associated with subbands successively crossing the Fermi level. This is seen in the three panels of Fig. 3, and is a geometrical effect typical of 1D that in the DOS leads to the multiple Van Hove singularities shown in Fig. 1(b). When superfluid gaps open in the single-particle excitation spectrum, there are no longer zero energy states available for charge excitations, and the singularities in the polarization bubble will be suppressed. The multiple peaks in the normal state polarization bubble will be significantly rounded by a sizeable smoothing of the momentum distribution that is induced by the large superfluid gaps. This rounding of the peaks is clearly seen in the results in Fig. 3. Interestingly, the superfluid state with large gaps shields the system against a Peierls instability typical of 1D materials. This is primarily due to the fact that the perfect nesting condition is no longer realizable in the presence at low energies of sufficiently large pairing gaps.

It should be noted, however, in the weak-coupled BCS regime where the superfluid gap is small compared with E_F, that screening becomes a strong effect, and in this regime screening suppresses the superfluidity. Thus we expect the unscreened approximation will break down for densities at which it predicts BCS superfluidity, and that the system will in fact remain in the normal state for those densities[9,26]. For this reason, we present results only in the BEC and crossover regimes.

In Eq. (1) we take the effective electron-hole pairing attraction $V_{\mathrm{e-h}}(q)$ to be the bare Coulomb interaction. For electrons and holes confined in nanoribbons of width W, separated by an insulating h-BN barrier of thickness d and dielectric constant $\kappa = 3$, we obtain[27],

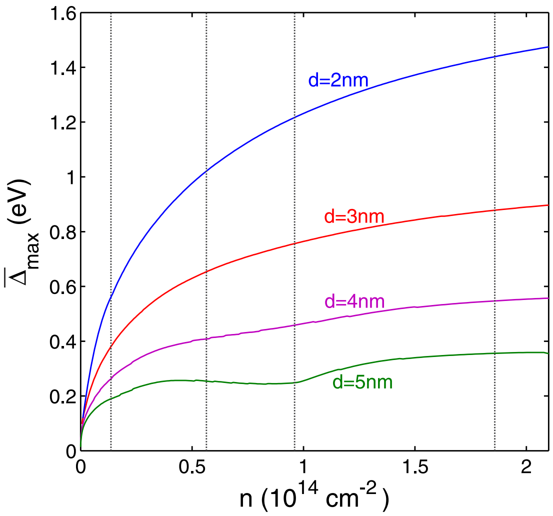

Figure 4. Maximum superfluid gap $\overline{\Delta}^{\max}$ averaged over the subbands for different thicknesses d of the insulating barrier separating the nanoribbons. Nanoribbon width is $W=2$ nm. Densities at which E_F enters the bottom of a new subband ε_j are indicated by the vertical dotted lines.

$$V_{\mathrm{e-h}}(q)=\frac{-2e^2}{\kappa W^2}\int_0^W\int_0^W dx'dxK_0(|q|\sqrt{(x-x')^2+d^2}). \tag{5}$$

One should in principle include in $V_{\mathrm{e-h}}(q)$, contributions from all inter-subband and intra-subband electron-hole scatterings, $v_{ijmn}(q)$, where i, j, m, n are the subband indices. However Fig. 1 of ref. 27, which plots $v_{ijmn}(q)$ for armchair graphene nanoribbons, shows that the intra-subband electron-hole scatterings, with $i-j=m-n=0$, dominate over all inter-subband scattering terms. In the small q limit, it is only the intra-subband scatterings that logarithmically diverge. For this reason, in Eq. (1) we may limit ourselves to the intra-subband contributions to the pairing interaction.

Results

Figure 4 shows the maximum superfluid gap $\overline{\Delta}^{\max}$ as a function of the density n, averaged over the multiple subbands of the nanoribbons, calculated using Eqs (1–5). $\overline{\Delta}^{\max}$ is the maximum value of the wave-vector dependent $\overline{\Delta}(k_y)$ averaged with respect to the subband index j. The nanoribbon width is $W=2$ nm, and d is the thickness of the insulating barrier. The densities at which the Fermi energy enters the bottom of a new subband $\varepsilon_j, j=1,2,\ldots$, are indicated by the vertical lines. The superfluid gap $\overline{\Delta}^{\max}$ is of the order of eV. It is interesting to note that in the low-density regime, $n\lesssim 10^{13}\,\mathrm{cm}^{-2}$, the maximum superfluid gap lies in the same range 200–20 meV predicted by Mohammadzadeh *et al.*[28] for the binding energy of excitons within a single nanoribbon. 2 $\overline{\Delta}^{\max}$ is a good estimate of the exciton binding energy when $|\mu|\ll E_F$. We note that the separation of the nanoribbons in our system is much less than the effective Bohr radius.

In Fig. 4 we notice a local boost in $\overline{\Delta}^{\max}$ near the minimum of each subband for barrier thickness $d=5$ nm. This boost arises from shape resonance effects associated with the van Hove singularities (Fig. 1(b)) and the quantum size effects in the pairing interaction. However, for thinner barriers $d\lesssim 4$ nm, where the electron-hole pairing becomes progressively stronger, the shape resonance effects are masked by a mixing of the subbands caused by the large superfluid gap. As $\overline{\Delta}^{\max}$ grows larger than the typical spacing between subbands, the system becomes decreasing less one-dimensional in character, thanks to the many channels available both for Cooper pairing and for forming the superfluid condensate.

Figure 5(a) shows the maximum superfluid gap $\Delta_j^{\max}$ for the separate subbands j as a function of n for nanoribbon width $W=2$ nm and barrier thickness $d=5$ nm. For comparison, the total Fermi energy E_F of the non-interacting nanoribbon system at density n is also shown. The vertical lines mark the densities at which E_F enters a new subband. For the lowest conduction subbands, there is a notable local boost in $\Delta_j^{\max}$ as E_F enters a new subband. This boost takes the form of a shape resonance in the superfluid gaps associated with a particular subband. However even for the lowest subbands, we lose some fine structure of the shape resonances because the gap mixes close subbands. Over the density range shown, the $\Delta_j^{\max}$ remain always of order E_F, and hence they lie in the strongly coupled regime.

Figure 5(b–d), show the momentum-dependence of the subband gaps $\Delta_j(k_y)$ for densities at which the chemical potential μ enters a new low-lying subband (marked in Fig. 5(a) by the vertical arrows). The peaks in $\Delta_j(k_y)$ are broad on the scale of $k_F=\pi/(2r_0)$, the inverse of the average inter-particle spacing, which confirms that we are in the BCS-BEC crossover regime of compact electron-hole pairs. In panels (c) and (d) of Fig. 5, the multiple peaks of $\Delta_j(k_y)$ are associated with the different Fermi energies of the subbands $(k_F)_j$, displaying a remaining fermionic character of the Cooper pairing in the BCS-BEC crossover regime.

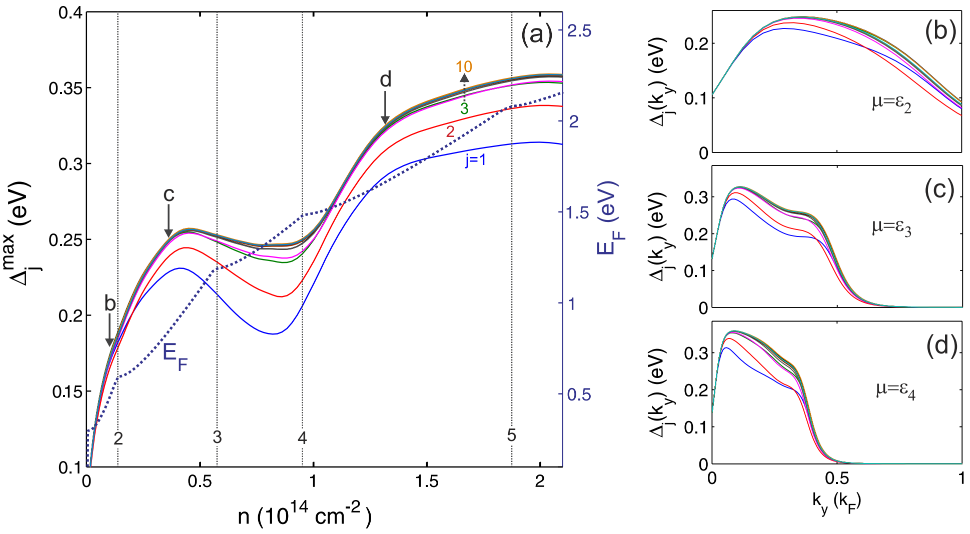

Figure 5. (**a**) Maximum superfluid gap Δ_j^{max} for subbands $j=1,2\ldots$ as function of density n. The dotted line shows the total Fermi energy E_F. Nanoribbon widths $W=2$ nm and barrier thickness $d=5$ nm. The densities at which E_F enters the bottom of a new subband are indicated by the vertical lines. Note that the Δ_j^{max} are all of order E_F. Right panels (**b–d**): momentum-dependent gaps $\Delta_j(k_y)$ for subbands j at densities marked by the arrows in panel (**a**) (at which $\mu=\varepsilon_2,\varepsilon_3,\varepsilon_4$).

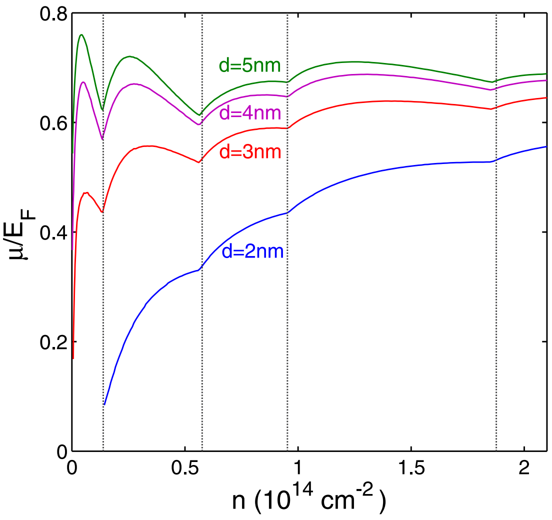

Figure 6. Ratio of chemical potential μ to Fermi energy E_F as function of density n for different values of the thickness d of the insulating barrier separating the nanoribbons. Nanoribbon width $W=2$ nm. The vertical dotted lines show the densities at which E_F enters the bottom of a subband.

Figure 6 shows the chemical potential μ as a function of density n for nanoribbon width $W=2$ nm and barrier thickness d. The μ is normalized to the corresponding Fermi energy of the non-interacting nanoribbon system at density n. The chemical potential is strongly renormalized with respect to the Fermi energy over the full range of n and d shown. When E_F enters a subband, μ has a dip. This is in contrast to the peak seen in the superfluid gap, and it is a shape antiresonance caused by the shape-resonance-generated peak in the gap. As d increases the pairing strength weakens, μ increases towards E_F and the shape (anti)resonances become sizeable, indicating that the system has entered the BCS-BEC crossover regime. This is particularly evident in Fig. 6 for $d=4-5$ nm. In the case of $d=2$ nm, $\mu \ll E_F$ and the shape (anti)resonances are completely smoothed out. This is a result of large superfluid gaps and it signals that the system is in the strong pairing BEC regime. When the density increases, the system always evolves towards the weaker pairing BCS regime for all values of d, with μ eventually arriving at E_F.

The average pair size of the Cooper pairs ξ_j in subband j is defined as the expectation value of the square of the relative coordinate of the Cooper pairs with respect to the square of the BCS wave function projected in the subband. This definition was originally introduced in ref. 29 to investigate the different regimes of pairing in high-T_c superconductivity in cuprates as a function of density. It has been extended to a multigap superconductor

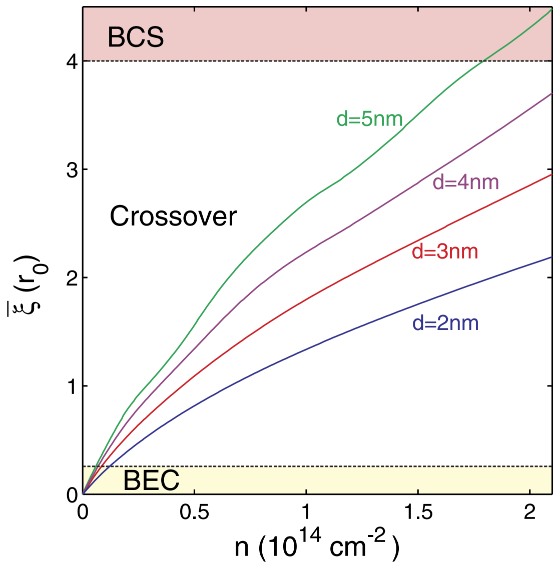

Figure 7. Pair correlation length $\bar{\xi}/r_0$ averaged over subbands as function of n, the carrier density for different values of the thickness d of the insulating barrier separating the nanoribbons. Nanoribbon width $W = 2$ nm.

throughout the BCS-BEC crossover in ref. 30 and to a multigap quasi-one-dimensional superfluid of ultracold fermions confined in cigar-shaped traps[31]. In wave-vector space,

$$\xi_j = \left[\frac{\sum_{k_y} \left| \nabla_{k_y} \left[u_j(k_y) v_j(k_y) \right] \right|^2}{\sum_{k_y} u_j^2(k_y) v_j^2(k_y)} \right]^{\frac{1}{2}}. \tag{6}$$

Figure 7 shows the pair correlation length $\bar{\xi}/r_0$ as a function of density normalized to the average inter-particle distance r_0. $\bar{\xi}/r_0$ is the partial average pair size for each subband averaged over the subbands. The nanoribbon width $W = 2$ nm. We designate $\bar{\xi}/r_0 < 0.25$ as the BEC regime, $0.25 < \bar{\xi}/r_0 < 4$ the BCS-BEC crossover regime, and $\bar{\xi}/r_0 > 4$ the BCS regime. As discussed, our approximation of neglecting screening is a good one for densities lying in the BCS-BEC crossover and BEC regimes. As expected, the density range for the strongly-coupled regime contracts with increasing barrier thickness d because the pairing becomes weaker.

We have neglected effects from impurities and disorder. We expect these effects to be small since while there is no direct information on impurity and disorder effects in graphene nanoribbons, but based on properties of analogous coupled electron-hole graphene monolayers, charge impurities concentrations up to $n_i < k_F/(\pi d)$ are not expected to destroy superfluidity[32]. At graphene-hBN interfaces, the charge impurity density $n_i \sim 10^{10}\,\mathrm{cm}^{-2}$ (see Ref. 33) so for $d \lesssim 5$ nm, the inequality is satisfied provided $n \lesssim 3 \times 10^6\,\mathrm{cm}^{-2}$. Since at density $n_i \sim 10^{10}\,\mathrm{cm}^{-2}$, the average spacing between charge impurities is orders of magnitude greater than the average spacing of the charge carriers, we do not expect our conclusions on screening to be affected by the presence of such impurities.

Conclusions

The superfluid gaps in our coupled electron-hole nanoribbon systems are large in absolute value and comparable to the Fermi energy. Both the quasi-one-dimensional confinement and the superfluid shape resonances due to quantum size effects play an important role here. The van Hove singularities in the density of states act non-linearly through the gap equation to significantly enhance the magnitude of the superfluid gaps. In the range of nanoribbon densities and barrier separations considered, we find that the electron-hole superfluid is for the most part in the strongly coupled pairing regime and that screening is strongly suppressed by the large superfluid gaps.

When the superfluid gaps are comparable to the subband energy separations, the gaps mix the subbands and this results in a rounding of the shape resonances. This effect is most pronounced for small separations between the nanoribbons where the electron-hole coupling is particularly strong. For larger separations, the electron-hole coupling is weaker and the superfluid gaps are smaller. This results in weaker subband mixing. When this is the case the shape resonances are sharper, which strengthens the local amplification of the gaps.

In our quasi-one-dimensional system there is no direct link between the superfluid transition temperature and the size of the superfluid gaps calculated within mean field. In our proposed device we find zero temperature superfluid gaps comparable to the Fermi energy, with gaps of order of hundreds of meV. Thus high transition temperature electron-hole superfluidity could be expected, with properties that are tuneable by changing the density. The device configurations we propose are experimentally realizable with current technologies. A superlattice formed of such nanoribbon devices could further stabilize the electron-hole superfluid phase over large areas.

References

1. Lozovik, Yu. E. & Yudson, V. I. Feasibility of superfluidity of paired spacially separated electrons and holes: a new superconductivity mechanism. *Pis′ma Zh. Eksp. Teor. Fiz.* **22,** 556–559 (1975) [*JETP Lett.* **22**, 274-276 (1975)].
2. Cartlidge, E. Graphene superconductivity seen. *Physics World* **28,** 10 (2015).
3. Gorbachev, R. V. *et al.* Strong Coulomb drag and broken symmetry in double-layer graphene. *Nature Phys.* **8,** 896–901 (2012).
4. Geim, A. K. & Grigorieva, I. V. Van der Waals heterostructures. *Nature* **499,** 419–425 (2013).
5. Mink, M. P., Stoof, H. T. C., Duine, R. A. & MacDonald, A. H. Influence of remote bands on exciton condensation in double-layer graphene. *Phys. Rev. B* **84,** 155409 (2011).
6. Min, H., Bistritzer, R., Su, J. & MacDonald, A. H. Room-temperature superfluidity in graphene bilayers. *Phys. Rev. B* **78,** 121401(R) (2008).
7. Bistritzer, R., Min, H., Su, J.-J. & MacDonald, A. H. Comment on "Electron screening and excitonic condensation in double-layer graphene systems". http://arxiv.org/abs/0810.0331v1 (2008).
8. Lozovik, Yu. E., Ogarkov, S. L. & Sokolik, A. A. Condensation of electron-hole pairs in a two-layer graphene system: Correlation effects. *Phys. Rev. B* **86,** 045429 (2012).
9. Perali, A., Neilson, D. & Hamilton, A. R. High-Temperature Superfluidity in Double-Bilayer Graphene. *Phys. Rev. Lett.* **110,** 146803 (2013).
10. Zarenia, M., Perali, A., Neilson, D. & Peeters, F. M. Enhancement of electron-hole superfluidity in double few-layer graphene. *Scientific Reports* **4,** 7319 (2014).
11. McCann, E. & Falko, V. I. Landau-Level Degeneracy and Quantum Hall Effect in a Graphite Bilayer. *Phys. Rev. Lett.* **96,** 086805 (2006).
12. Min, H. & MacDonald, A. H. Chiral decomposition in the electronic structure of graphene multilayers. *Phys. Rev. B* **77,** 155416 (2008).
13. Lin, Y. *et al.* 100-GHz Transistors from Wafer-Scale Epitaxial Graphene. *Science* **327,** 662 (2010).
14. Dimiev, A. *et al.* Low Loss, High Permittivity Composites Made from Graphene Nanoribbons. *ACS Appl. Mater. Interfaces* **3,** 4657–4661 (2011).
15. Dimiev, A. M. *et al.* Permittivity of dielectric composite materials comprising graphene nanoribbons, The effect of nanostructure. *ACS Appl. Mater. Interfaces* 5, 7567–7573 (2013).
16. Li, L., Raji, A.-R. O. & Tour, J. M. Graphene-Wrapped MnO_2-Graphene Nanoribbons as Anode Materials for high performance lithium batteries. *Adv. Mater.* **25** 6298–6302 (2013).
17. Han, M. Y., Özyilmaz, B., Zhang, Y. & Kim, Ph. Energy Band-Gap Engineering of Graphene Nanoribbons. *Phys. Rev. Lett.* **98,** 206805 (2007).
18. Cai, J. *et al.* Atomically precise bottom-up fabrication of graphene nanoribbons. *Nature* **466,** 470–473 (2010).
19. Perali, A., Bianconi, A., Lanzara, A. & Saini, N. L. The gap amplification at a shape resonance in a superlattice of quantum stripes: A mechanism for high T_c. *Solid State Commun.* **100,** 181–186 (1996).
20. Bianconi, A., Valletta, A., Perali, A. & Saini, N. L. High T_c superconductivity in a superlattice of quantum stripes. *Solid State Commun.* **102,** 369–374 (1997).
21. Bianconi, A., Valletta, A., Perali, A. & Saini, N. L. Superconductivity of a striped phase at the atomic limit. *Physica C* **296,** 269–280 (1998).
22. Shanenko, A. A., Croitoru, M. D., Zgirski, M., Peeters, F. M. & Arutyunov, K. Size-dependent enhancement of superconductivity in Al and Sn nanowires: Shape-resonance effect. *Phys. Rev. B* **74,** 052502 (2006).
23. Brey, L. & Fertig, H. A. Electronic states of graphene nanoribbons studied with the Dirac equation *Phys. Rev. B* **73,** 235411 (2006).
24. Abergel, D. S. L. Excitonic condensation in spatially separated one-dimensional systems. *Appl. Phys. Lett.* **106,** 213103 (2015).
25. Pieri, P., Neilson, D. & Strinati, G. C. Effects of density imbalance on the BCS-BEC crossover in semiconductor electron-hole bilayers. *Phys. Rev. B* **75,** 113301 (2007).
26. Maezono, R., Ríos, P. L., Ogawa, T. & Needs, R. J. Excitons and biexcitons in symmetric electron-hole bilayers. *Phys. Rev. Lett.* **110,** 216407 (2013).
27. Brey, L. & Fertig, H. A. Elementary electronic excitations in graphene nanoribbons. *Phys. Rev. B* **75,** 125434 (2007).
28. Mohammadzadeh, L., Asgari, A., Shojaei, S. & Ahmadi, E. Theoretical calculation of excitonic binding energies and optical absorption spectra for Armchair graphene nanoribbons. *Eur. Phys. J.* **84,** 249 (2011).
29. Pistolesi, F. & Strinati, G. C. Evolution from BCS superconductivity to Bose condensation: role of the parameter $k_F\xi$. *Phys. Rev. B* **49,** 6356 (1994).
30. Guidini, A. & Perali, A. Band-edge BCS-BEC crossover in a two-band superconductor: physical properties and detection parameters. *Supercond. Sci. Technol.* **27,** 124002 (2014).
31. Shanenko, A. A. *et al.* Atypical BCS-BEC crossover induced by quantum-size effects. *Phys. Rev. A* **86,** 033612 (2012).
32. Bistritzer, R. & MacDonald, A. H. Influence of Disorder on Electron-Hole Pair Condensation in Graphene Bilayers. *Phys. Rev. Lett.* **101,** 256406 (2008).
33. Martin, J. *et al.* Observation of electron-hole puddles in graphene using a scanning single-electron transistor. *Nature Phys.* **4,** 144–148 (2008).

Acknowledgements

M.Z. acknowledges support by the Flemish Science Foundation (FWO-Vl), the University Research Fund (BOF), and the European Science Foundation (POLATOM). A.P. and D.N. acknowledge support by the University of Camerino FAR project CESEMN. The authors thank the colleagues involved in the MultiSuper International Network (http://www.multisuper.org) for exchange of ideas and suggestions for this work.

Author Contributions

D.N., F.M.P. and A.P. conceived the idea. D.N. and A.P. supervised the project. D.N. and A.P. designed the calculation, and M.Z. carried out the calculation. All authors contributed to the analysis and interpretation of the results, and all authors wrote the paper.

Additional Information

Competing financial interests: The authors declare no competing financial interests.

How to cite this article: Zarenia, M. *et al.* Large gap electron-hole superfluidity and shape resonances in coupled graphene nanoribbons. *Sci. Rep.* **6**, 24860; doi: 10.1038/srep24860 (2016).

This work is licensed under a Creative Commons Attribution 4.0 International License. The images or other third party material in this article are included in the article's Creative Commons license, unless indicated otherwise in the credit line; if the material is not included under the Creative Commons license, users will need to obtain permission from the license holder to reproduce the material. To view a copy of this license, visit http://creativecommons.org/licenses/by/4.0/